MATER. RES. LETT.
2019, VOL. 7, NO. 2, 47–52
https://doi.org/10.1080/21663831.2018.1553801

MATERIALS RESEARCH LETTERS
Taylor & Francis
Taylor & Francis Group

ORIGINAL REPORT

Graphene-coated tungsten nanowires deliver unprecedented modulus and strength

Zhong-Wei Hu[a], Min Wang[a], Chao-Wei Guo[a], Zhi-Wei Shan[a], Ju Li[a,b,c] and Wei-Zhong Han[a]

[a]Center for Advancing Materials Performance from the Nanoscale (CAMP-Nano) & Hysitron Applied Research Center in China (HARCC), State Key Laboratory for Mechanical Behavior of Materials, Xi'an Jiaotong University, Xi'an, People's Republic of China; [b]Department of Nuclear Science and Engineering, Massachusetts Institute of Technology, Cambridge, MA, USA; [c]Department of Materials Science and Engineering, Massachusetts Institute of Technology, Cambridge, MA, USA

ABSTRACT

Tungsten (W) nanowires have a wide range of chemical, electronic, and mechanical applications. However, the modulus and strength of traditional W nanowires are quite low, and how to improve their mechanical performance remains a challenge. Here, we describe a novel graphene-coated W nanowires that demonstrate a Young's modulus of 885 GPa (twice that of W) and a fracture strength of up to 24.7 GPa (66% of the ideal strength). Both the Young's modulus and the fracture strength show a strong size effect, resulting from the graphene-nanowire core–shell structure.

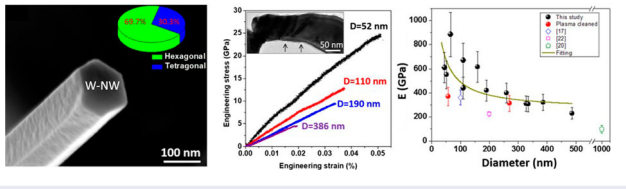

IMPACT STATEMENT

We report a novel graphene-coated W nanowires that demonstrate unprecedented Young's modulus (885 GPa, twice that of W) and fracture strength (24.7 GPa, 66% of the ideal strength).

ARTICLE HISTORY
Received 14 July 2018

KEYWORDS
W nanowires; graphene; Young's modulus; fracture strength; size effect

1. Introduction

Metallic nanowires are promising building blocks for a host of applications such as transparent electrodes, sensors, flexible or stretchable electronics, etc. [1–7]. The operation and reliability of nanowires-based devices call for a robust mechanical performance and a thorough understanding of their deformation behaviors. Tungsten (W) nanowires have been used in a number of electronic and mechanical applications because of their outstanding field-emission characteristics and usefulness as pH sensitive electrodes etc. [8–11]. The behavior and reliability of W nanowires while performing these functions depend on their mechanical properties, which are expected to be different from their bulk counterparts because of the increased surface-to-volume ratio.

W nanowires have been successfully fabricated by using chemical vapor deposition [12–15] or by electrochemical etching of a eutectic W alloy [16]. However, investigations of the mechanical properties of W nanowires have been scarce and this field has remained largely unexplored [17–24]. Moreover, the Young's modulus and fracture strength of traditional W nanowires are significantly lower than the expected values [17–24], while the underlying mechanisms that cause poor mechanical performance remain elusive. The Young's modulus of W nanowires with diameters of 100–300 nm is only 332 GPa, which is lower than the bulk modulus (411 GPa) [17]. In addition, the Young's modulus and hardness of W microwhiskers (10–20 μm in diameter) were also studied by nanoindentation; again, a very low modulus of 270 GPa was obtained [19]. The hardness of W microwhiskers (8.63 GPa) is higher than that of W, while the modulus is only two-thirds of the bulk modulus [19]. Recently, the mechanical properties of W nano-pillars were measured by *in situ* tensile [21]. The W nano-pillars show a strong size-dependent

CONTACT Wei-Zhong Han wzhanxjtu@mail.xjtu.edu.cn Center for Advancing Materials Performance from the Nanoscale (CAMP-Nano) & Hysitron Applied Research Center in China (HARCC), State Key Laboratory for Mechanical Behavior of Materials, Xi'an Jiaotong University, Xi'an 710049, People's Republic of China

strength, however, the maximum strength of W nano-pillars is 2.5 GPa, which is only 6.25% of the ideal strength of W [21]. Furthermore, the Young's modulus of W nano-pillars is less than 100 GPa [21]. The traditional W nanostructures-though they fall into the nanoscale regime-display low Young's modulus and limited strength. The inferior mechanical performance of W nanowires is likely caused by surface contamination, such as oxidation, carbonization, etc., or by flaws introduced during fabrication [25,26]. In order to improve the performance of W-nanowire-based devices, new strategies need to be developed to overcome the poor mechanical properties of W nanowires.

Here, we report a novel graphene-coated W nanowires (G-W-NWs). Graphene, with Young's modulus of more than 1 TPa and an intrinsic strength of 130 GPa, has been reported as the strongest materials ever measured [27]. As a result, the G-W-NWs deliver extraordinary Young's modulus and fracture strength.

2. Experimental methods

G-W-NWs were synthesized by chemical vapor deposition, using Ni nanoparticles as catalysts and WO_3 as the reactant. The fabrication was performed in a hydrogen atmosphere at 850°C, as illustrated in Figure S1. Previously, graphene has been successfully synthesized on W surface under similar synthesis conditions [28]. Therefore, the nanowires are likely covered by graphene. The morphologies and structures of as-synthesized nanowires were characterized by scanning electron microscopy (SEM), transmission electron microscopy (TEM), and Raman spectroscopy. Some of the nanowires were transferred and placed on the 'push-to-pull' (PTP) micromechanical devices (see Figure S2) to conduct *in situ* tensile tests, using a Hysitron PicoIndenter (PI 95) inside a FEG JEOL 2100F TEM (200 kV) with a displacement control mode. The displacement rate was programed to be 10 nm/s in tension, which corresponds to a strain rate of about 1×10^{-3} s^{-1}.

3. Results and discussion

Figure 1(a) is a typical SEM image of the high density of nanowire grown on a (100) silicon substrate. The diameters of the nanowire range from 45 to 500 nm. The statistical distribution of the length of the nanowires is shown in Figure 1(b). Most of the nanowires are longer than 10 μm, and they are long enough for *in situ* tensile testing. The SEM images of the heads of the nanowire reveal that the cross-sections are mostly hexagonal or tetragonal (Figure 1(c)), with a statistical ratio of about

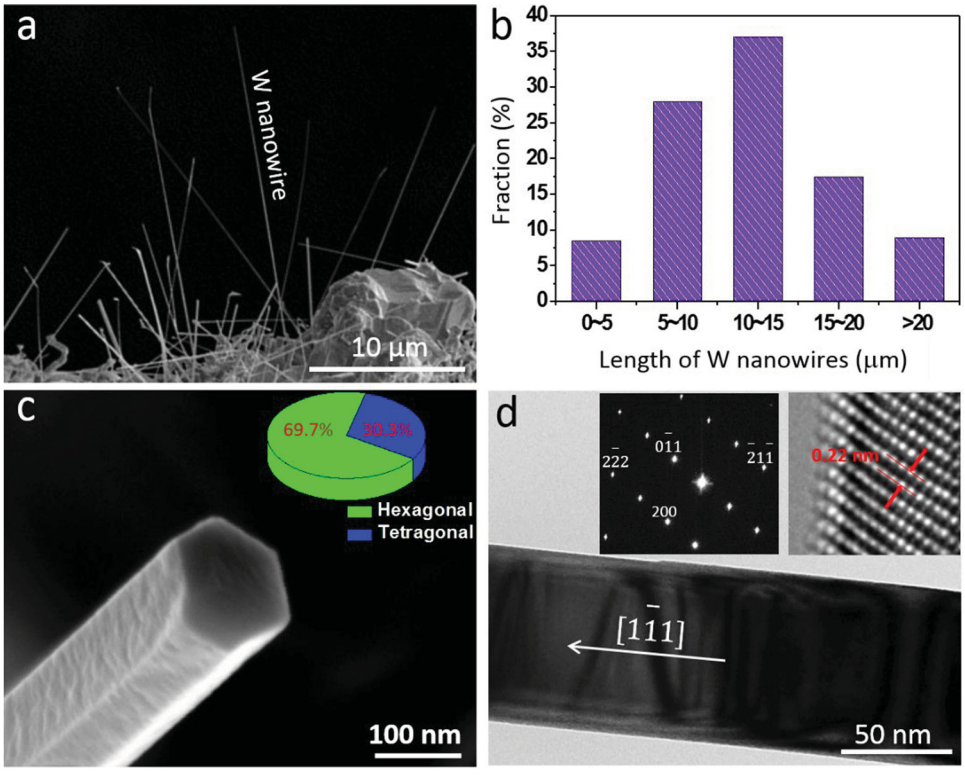

Figure 1. (a) SEM image of the as-grown nanowire; (b) length distribution of W nanowires. (c) Typical hexagonal cross-section of W nanowires. The inset pie chart shows the ratio of nanowires with cross-section of hexagonal versus tetragonal. (d) TEM image of a single W nanowire.

7:3. Figure 1(d) displays the typical TEM image of the edge of a nanowire with diameter of 80 nm. The nanowire is straight and has a uniform cross-section. The growth direction of nanowire is [1$\bar{1}$1]. High-resolution TEM from the edge of nanowire indicates that it is body-centered cubic single crystals.

To further probe the surface structure of nanowires, Raman microscopy was performed using a 532 nm laser beam on an individual nanowire. As shown in Figure 2, a clear G peak appears at 1570 cm^{-1} on the Raman scan, indicating that graphene layers were formed on the surface of the nanowire [29,30]. In addition, a D peak and a wide 2D peak were also identified at 1392 and 2939 cm^{-1} on the Raman scan, revealing that these are somewhat defective multilayer graphene structures [29,30]. In order to make a comparison, we purged the surface of some of the G-W-NWs by using plasma cleaning [31]; and then studied the surface structures again. The characteristic peaks of graphene have disappeared, as shown in Figure 2. In addition, the thickness of the surface carbon layer was also reduced significantly (Figure S3), indicating that the plasma cleaning removed the surface graphene layers [30]. The above results suggest that the nanowires synthesized in our experiments are coated with multilayers of graphene.

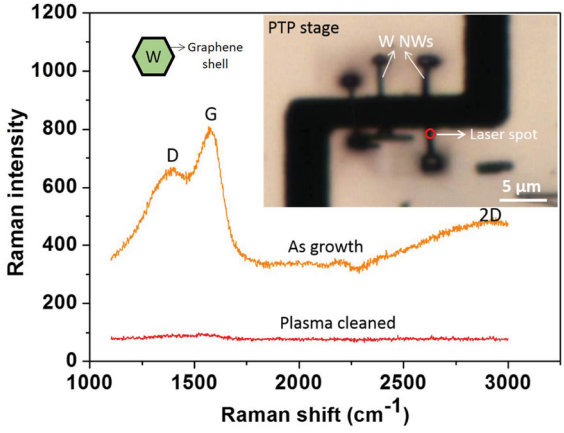

Figure 2. The yellow line is the Raman shift of an as-grown nanowire, and the red line is the Raman shift of the same nanowire after plasma cleaning for 30 min. The insets show that the PTP stage was used for Raman microscopy and the core–shell structures of nanowire.

In order to explore the mechanical performance of the G-W-NWs, we performed *in situ* mechanical tensile test. Figure 3(a) shows a single nanowire with a length of 12.5 μm, which was welded onto the PTP stage. Figure 3(b) shows the typical engineering stress–strain curve of four G-W-NWs with different diameters. A typical *in situ* tensile test of the nanowire is shown in Movie S1. All these nanowires display a large and obvious elastic deformation stage, then fracture abruptly with negligible plastic strain. The elastic modulus, fracture strength, and fracture strain of the nanowires demonstrate a strong size-dependent behavior. The fracture strength increases from 4.5 GPa (D = 386 nm) to 24.7 GPa (D = 52 nm). The slope of the engineering stress–strain curves reflects

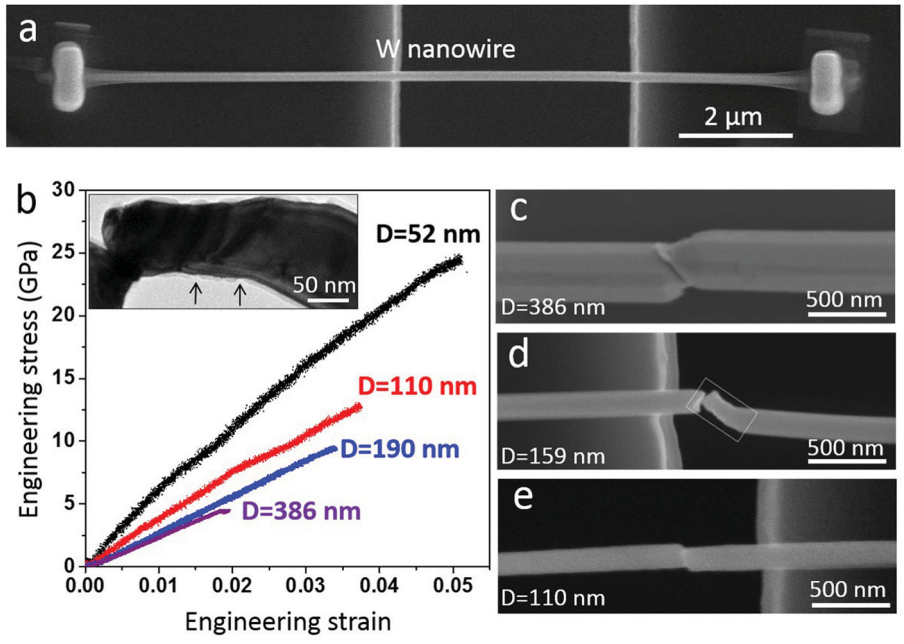

Figure 3. (a) SEM image of a well-aligned nanowire. (b) Typical engineering stress–strain curve of four nanowires with different diameters. (c–e) Fracture features of nanowires taken after tensile tests. The inset in b is the TEM image of the necking part of the nanowire in d.

the variation of the elastic modulus of nanowires, which is increased significantly by decreasing their diameter. The elastic modulus of nanowire with a diameter of 52 nm is 885 GPa, which is more than twice the elastic modulus of bulk W, and larger than the elastic modulus of all other nanowires [17–24]. After the tensile tests, most of the fractured nanowires ricocheted off the PTP stage, and only a few of them remained. Figure 3(c–e) shows typical SEM images of the fractured nanowires. Obvious necking features and drastic plastic deformation were only identified around the fracture front. Figure 3(c) shows failure feature of a faceted nanowire with a diameter of 386 nm; an obvious shear fracture mode can be identified. The fracture character of a nanowire with a diameter of 159 nm was also captured; local severe stretching and bending occurred around the fracture head, as shown in Figure 3(d). The necking part of the nanowire displays obvious deformation steps at the side surface, as marked in the inset in Figure 3(b). The carbon shell cracked into grooves, which are likely formed by dislocation cutting graphene layer. Figure 3(d) shows the failure of a nanowire with a diameter of 110 nm. It also underwent a localized shear deformation before fracture. These G-W-NWs demonstrate extraordinary elastic deformation and a very localized plastic deformation. Such a deformation behavior is significantly different from that of the traditional W nano-pillars in which a global plasticity sets in first, followed by strain localization and failure [21,32,33]. The deformation feature of nanowires is due to the strong confinement of the graphene layers.

To further explore the size-dependent behavior of G-W-NWs, a group of 12 nanowires with diameters ranging from 45 to 486 nm were tested. Figure 4(a) shows the Young's modulus of the G-W-NWs varied as a function of their diameter, and compares with the elastic modulus of traditional nanowires [17,20,22]. The method for calculation of the Young's modulus and the error bars are discussed in supplementary materials. We adopted two methods to measure the strain of nanowires: one is to put markers on the nanowires, then track the changes of the markers; the other one is to monitor the variation of the gap of the PTP stage. Based on these two methods, we have corrected the strain of nanowires. A clear validation of the 'smaller is stronger' rule can be found in the G-W-NWs. The highest Young's modulus for a G-W-NW with diameter of 50 nm can be as high as 885 GPa, which is twice of the modulus of W. In order to identify the effect of the surface graphene layer on the elastic properties of nanowires, we tested two of the nanowires purged by plasma cleaning; these are the two red data points shown in Figure 4(a). After plasma cleaning, the surface graphene layers were destroyed (Figure 2 and Figure S3). Therefore, the Young's modulus of the two plasma-cleaned nanowires was significantly smaller than that of the G-W-NWs with similar diameter, indicating the strong effect of graphene on the stiffness of nanowires.

The size-dependent Young's modulus of G-W-NWs can be explained by the classical model for core–shell nanowires [33]. The variation of the Young's modulus of G-W-NWs as a function of their diameter can be expressed as

$$E = E_w\left[1+8\left(\frac{E_g}{E_w}-1\right)\left(\frac{r_g}{D}-3\frac{r_g^2}{D^2}+4\frac{r_g^3}{D^3}-2\frac{r_g^4}{D^4}\right)\right] \quad (1)$$

where E_w is the Young's modulus of the W, E_g is the Young's modulus of graphene layer, r_g is the thickness of the graphene layer, and D is the diameter of the nanowires. Equation (1) was used to fit the experimental results, and the fitting curve is shown in Figure 4(a). In general, the model can reasonably predict the Young's modulus of G-W-NWs. The optimized curve fitting yields the following values for the three parameters, E_w =259 GPa, E_g =1311 GPa, and r_g =3.06 nm. The fitted Young's modulus of graphene is comparable to the values measured in previous experiments [26]. However, the Young's modulus of larger nanowires (> 500 nm)

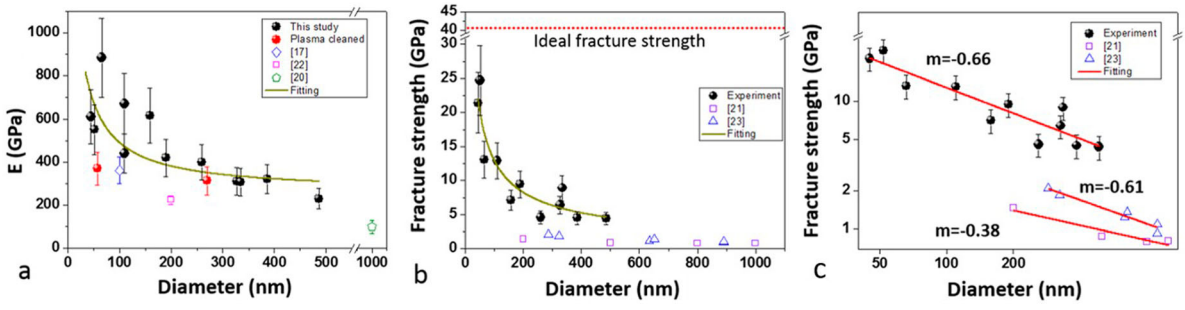

Figure 4. (a) Variation of the Young's modulus of G-W-NWs as a function of their diameter. (b) Fracture strength of G-W-NWs continuously increases with the reduction of the diameter. The green lines are added for legibility only. (c) A log–log plot of the fracture strength of G-W-NWs versus their diameter.

is still significantly lower than the bulk modulus of W. We have examined the chemical composition of the cross-section of these nanowires, as shown in Figure S4. Significant oxidation and carbonation are detected, which are the origin of the low elastic modulus [25]. According to the calculated thickness of the graphene shell (r_g =3.06 nm), roughly 7–8 layers of graphene were formed on the nanowires, consistent with the Raman scan in Figure 2. These results indicate that the graphene layer raises the Young's modulus of nanowire significantly.

In addition to the unprecedented Young's modulus, the G-W-NWs also exhibit ultrahigh fracture strength. Figure 4(b) shows the measured fracture strength of all the tested NWs as a function of diameter, and compares with other studies [17–24]. The fracture strength of the G-W-NWs is higher than all other W nano-pillars (see Figure 4(b)) [17–24]. In addition, the fracture strength of nanowire has a strong size effect due to the continuous increase of the volume fraction of the graphene layers with reducing the diameter of the sample. The fracture strength increases from 4.4 GPa to 24.7 GPa when the diameter decrease from 486 nm to 45 nm. The highest fracture strength of the nanowires equals 66% of the theoretical strength of W along the [111] direction [24]. By fitting the fracture strength using the rule of mixtures (Figure S7), the strength of the graphene layer is found to be 83.4 GPa, which is smaller than the intrinsic strength of a single layer of graphene, indicating the defective multilayer structure of graphene in this case (Figure 2). The W core has a strength of 3.1 GPa, which is higher than that of the W nano-pillars [21]. The size effect of these nanowires can be plotted on a log–log scale, and a power law exponent factor of about $m = -0.66$ can be obtained, which is higher than the observed size effect in traditional W nano-pillars [21–23], as shown in Figure 4(c).

The size effect of Young's modulus and fracture strength of metallic nanowires has been widely reported; however, our current results contradict the results of previous investigations [34–39]. In general, the size effect of the elastic modulus comes from the different properties of the surface layer and the internal core. For oxide nanowires, the surface stress/surface energy effect is the reason for size-dependent modulus [34–36]. While for metallic nanowires, a size-independent Young's modulus is widely reported except for the silver and lead nanowires [36–39]. Notably, the current study shows that a thin layer of graphene covering the W nanowires induces a strong size effect in both Young's modulus and fracture strength. This is similar to the situation of Al nano-pillars covered with a thin layer of native oxide [39]. The brittle fracture behavior of G-W-NWs in our experiments is also different from the deformation behaviors of traditional nanowires, which show large plastic deformation and local superelasticity [23,24,32,33]. The strong confinement imposed by the graphene layers suppresses the surface dislocation nucleation, thus leading to a huge elastic deformation stage before final localized catastrophic fracture.

4. Conclusions

G-W-NWs with [111] growth direction have been fabricated. The Young's modulus of G-W-NWs shows a stiffening tendency at reduced diameters, and a remarkably high Young's modulus of 885 GPa can be obtained. The fracture strength of the G-W-NWs also increases with decreasing diameters, and a fracture strength as high as 24.7 GPa can be obtained. The current strategy can be deliberately designed to fabricate graphene-coated nanowires or nanostructures with fine-tuned electronic, chemical, and mechanical properties.

Acknowledgement

Z. W. H appreciated Mrs P. J. Y, X. G. W, Y. Q. Z and Dr Y. B. Q for kind assistances.

Disclosure statement

No potential conflict of interest was reported by the authors.

Funding

This work was supported by the National Key R&D Program of China (2017YFB0702301), the National Natural Science Foundation of China (51471128 and 51621063), and the 111 Project of China (BP2018008).

References

[1] Pascual JI, Méndez J, Gómez-Herrero J, et al. Properties of metallic nanowires: from conductance quantization to localization. Science. 1995;267:1793–1795.
[2] Smith PA, Nordquist CD, Jackson TN, et al. Electric-field assisted assembly and alignment of metallic nanowires. Appl Phys Lett. 2000;77:1399–1401.
[3] Atashbar MZ, Singamaneni S. Room temperature gas sensor based on metallic nanowires. Sens Actuat B-Chem. 2005;111–112:13–21.
[4] Li Y, Qian F, Xiang J, et al. Nanowire electronic and optoelectronic devices. Mater Today. 2006;9:18–27.
[5] Lee JY, Connor ST, Cui Y, et al. Solution-processed metal nanowire mesh transparent electrodes. Nano Lett. 2008;8:689.
[6] Lee S, Shin S, Lee S, et al. Stretchable electronics: Ag nanowire reinforced highly stretchable conductive fibers for wearable electronics. Adv Funct Mater. 2015;25:3105–3105.

[7] Cheng GM, Yin S, Chang TH, et al. Anomalous tensile detwinning in twinned nanowires. Phys Rev Lett. 2017;119:256101.
[8] Mullendore JA, Pegher, SM. Tungsten penetrator. US5064462(P), 1991.
[9] Fenster C, Smith AS, Abts A, et al. Single tungsten nanowires as pH sensitive electrodes. Electrochem Commun. 2008;10:1125–1128.
[10] Wang SL, He YH, Fang XS, et al. Structure and field-emission properties of sub-micrometer-sized tungsten-whisker arrays fabricated by vapor deposition. Adv Mater. 2009;21:2387–2392.
[11] Choi J, Kim J. Highly sensitive hydrogen sensor based on suspended, functionalized single tungsten nanowire bridge. Sens Actuat B-Chem. 2009;136:92–98.
[12] Starliper AG, Kenworthy H. Tungsten whiskers by vapor-phase growth. Electrodepos Surf Treat. 1974;2:249–262.
[13] Vaddiraju S, Chandrasekaran H, Sunkara MK. Vapor phase synthesis of tungsten nanowires. J Am Chem Soc. 2003;125:10792–10793.
[14] Wang SL, He YH, Zou J, et al. Catalytic growth of metallic tungsten whiskers based on the vapor-solid-solid mechanism. Nanotechnology. 2008;19:345604.
[15] Liu GY, Song M, Liu XL, et al. Factors affecting the growth of micro/nano-sized tungsten whiskers synthesised by vapour deposition. Philos Mag. 2013;93:584–597.
[16] Hassel AW, Smith AJ, Milenkovic S. Nanostructures from directionally solidified NiAl-W eutectic alloys. Electrochim Acta. 2006;52:1799–1804.
[17] Cimalla V, Röhlig CC, Pezoldt J, et al. Nanomechanics of single crystalline tungsten nanowires. J Nanomater. 2008;1:145–152.
[18] Skotnicová K, Kirillova VM, Zaporozhets OI, et al. Investagation of physical properties of tungsten-based single crystals using an ultrasonic method. Mater Technol. 2014;48:823–826.
[19] Huang H, Wu YQ, Wang SL, et al. Mechanical properties of single crystal tungsten microwhiskers characterized by nanoindentation. Mater Sci Eng A. 2009;523:193–198.
[20] Pugachevskii MA. Determining elastic moduli of tungsten nanowires. Tech Phys Lett. 2010;36:639–641.
[21] Kim JY, Jang D, Greer JR. Tensile and compressive behavior of tungsten, molybdenum, tantalum and niobium at the nanoscale. Acta Mater. 2010;58:2355–2363.
[22] Hou LZ, Wang SL, Chen GL, et al. Mechanical properties of tungsten nanowhiskers characterized by nanoindentation. Trans Nonferr Metal Soc China. 2013;23:2323–2328.
[23] Cui YN, Po G, Ghoniem N. Temperature insensitivity of the flow stress in body-centered cubic micropillar crystals. Acta Mater. 2016;108:128–137.
[24] Šob M, Wang LG, Vitek V. Theoretical tensile stress in tungsten single crystals by full-potential first-principles calculations. Mater Sci Eng A. 1997;234:1075–1078.
[25] Wang SL, Chen GL, Huang H, et al. Vapor-phase synthesis, growth mechanism and thickness-independent elastic modulus of single-crystal tungsten nanobelts. Nanotechnology. 2013;24:505705.
[26] Kiener D, Motz C, Rester M, et al. FIB damage of Cu and possible consequences for miniaturized mechanical tests. Mater Sci Eng A. 2007;459:262–272.
[27] Lee CG, Wei XD, Kysar JW, et al. Measurement of the elastic properties and intrinsic strength of monolayer graphene. Science. 2008;321:385–388.
[28] Zou ZY, Song XJ, Chen K, et al. Uniform single-layer graphene growth on recyclable tungsten foils. Nano Res. 2015;8:592–599.
[29] Ferrari AC, Meyer JC, Scardaci V, et al. Raman spectrum of graphene and graphene layers. Phys Rev Lett. 2006;97:187401.
[30] Dresselhaus MS, Jorio A, Hofmann M, et al. Perpectives on carbon nanotubes and graphene Raman spectroscopy. Nano Lett. 2010;10:751–758.
[31] Peltekis N, Kumar S, McEvoy N, et al. The effect of downstream plasma treatments on graphene surfaces. Carbon N Y. 2012;50:395–403.
[32] Li SZ, Ding XD, Li J, et al. High-efficiency mechanical energy storage and retrieval using interfaces in nanowires. Nano Lett. 2010;10:1774–1779.
[33] Wang JW, Zeng Z, Weinberger CR, et al. In situ atomic-scale observation of twinning-dominated deformation in nanoscale body-centred cubic tungsten. Nature Mater. 2015;14:594–600.
[34] Chen CQ, Shi Y, Zhang YS, et al. Size dependence of Young's modulus in ZnO nanowires. Phys Rev Lett. 2006;96:075505.
[35] Cuenot S, Frétigny C, Champagne SD, et al. Surface tension effect on the mechanical properties of nanomaterials measured by atomic force microscopy. Phys Rev B. 2004;69:165410.
[36] Wang GF, Li XD. Predicting Young's modulus of nanowires from first-principles calculations on their surface and bulk materials. J Appl Phys. 2008;104:113517.
[37] Wu B, Heidelberg A, Boland JJ. Mechanical properties of ultrahigh-strength gold nanowires. Nature Mater. 2005;4:525–529.
[38] Zhu Y, Qin QQ, Xu F, et al. Size effects on elasticity, yielding, and fracture of silver nanowires: in situ experiments. Phys Rev B. 2012;85:045443.
[39] Li SH, Han WZ, Li J, et al. Small-volume aluminum alloys with native oxide shell deliver unprecedented strength and toughness. Acta Mater. 2017;126:202–209.